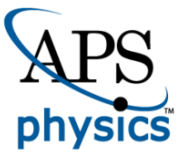

Jamming Distance Dictates Colloidal Shear Thickening

Shravan Pradeep, Mohammad Nabizadeh, Alan R. Jacob, Safa Jamali, and Lilian C. Hsiao

Phys. Rev. Lett. **127**, 158002 — Published 6 October 2021

DOI: 10.1103/PhysRevLett.127.158002

Jamming Distance Dictates Colloidal Shear Thickening

Shravan Pradeep[1], Mohamad Nabizadeh[2], Alan R. Jacob[1], Safa s[2], and Lilian C. Hsiao[1,*]

[1] Department of Chemical and Biomolecular Engineering, North Carolina State University, Raleigh, North Carolina – 27695, USA

[2]Department of Mechanical and Industrial Engineering, Northeastern University, Boston, Massachusetts – 02115, USA

[*] Corresponding author: lilian_hsiao@ncsu.edu

Abstract

We report experimental and computational observations of dynamic contact networks for colloidal suspensions undergoing shear thickening. The dense suspensions are comprised of sterically stabilized poly(methyl methacrylate) colloids that are spherically symmetric and have varied surface roughness. Confocal rheometry and dissipative particle dynamics simulations show that the shear thickening strength β scales exponentially with the scaled deficit contact number and the scaled jamming distance. Rough colloids, which experience additional rotational constraints, require an average of 1.5 - 2 fewer particle contacts as compared to smooth colloids, in order to generate the same β. This is because the surface roughness enhances geometric friction in a way that the rough colloids do not experience a large change in the free volume near the jamming point. The available free volume for different colloid roughness is related to the deficiency from the maximum number of nearest neighbors at jamming under shear. Our results further suggest that the force per contact is different for particles with different morphologies.

Dense suspensions of colloidal particles with stochastic Brownian motion exhibit shear thickening under flow, a non-Newtonian behavior where the suspension viscosity η increases mildly or strongly depending on the applied shear stress σ and particle volume fraction ϕ. The ability to design the onset of shear thickening σ^* provides a unique advantage in the reversible tuning of material mechanics, which is of great interest in fields such as soft robotics, impact resistant fabrics, and liquid manufacturing [1-3]. However, the tunability in these systems currently remains at a rudimentary level of "on" or "off". For dense suspensions to truly advance technology, the level of control over the shear thickening needs to become more deliberate and refined [4,5]. In this manuscript, we show that designing shear thickening strength is possible for a broad class of colloidal suspensions through a singular parameter: the distance to jamming.

A jammed material at ϕ_J is conventionally defined as a disordered particulate system that has developed a yield stress [6]. Shear thickening shares similarities to jamming in that the particles in a flowing suspension become impeded by the nearest neighbors that they require an increasing amount of stress to continue flowing [1,7]. The microstructural origin of shear thickening was first attributed to the formation of hydroclusters in the Stokesian Dynamics simulations [8]. Experiments later corroborated this observation [9], suggesting that the shear thickening onset can be discussed through a single dimensionless parameter, the Péclet number ($Pe_{sh} = 6\pi\eta a_{eff}^3 \dot{\gamma} / k_B T$), that represents the ratio of hydrodynamic to thermal forces acting on colloids. More recently, simulations that incorporate explicit interparticle friction μ or particle roughness plus lubrication hydrodynamics were able to fully capture the large increase in viscosity that is characteristic of strong shear thickening [10,11]. An important result from these simulations is the appearance of space-spanning force chains and velocity correlations in shear thickened suspensions [12]. These force chains arise from any combination of σ- and ϕ-based constraints including hydrodynamics,

repulsion, adhesion, and solid contact friction [11,13,14]. As Pe_{sh} increases, the force chains proliferate and grow stronger as a system undergoes stronger shear thickening and ultimately shear jamming [15]. Interestingly, conventional microstructural characterization techniques such as the radial distribution function [14] or scattering patterns in the velocity-gradient-vorticity planes [16] are not sensitive to differences between shear thickened states. As $\phi \rightarrow \phi_J$ and σ increases, conservation laws state that the contact distance between particles in a constant-volume suspension must decrease, leading to a greater number of contacts. To address a lack of experimental evidence of contacts chains in the literature, we focus on microstructural characterization of the dynamic contact networks formed by dense colloidal suspensions in shear thickening flows.

We use the mean contact number $\langle z \rangle$, a measure for the number of contacting nearest neighbors around particles, to quantify the suspension microstructure because of the strong correlation of $\langle z \rangle$ with bulk mechanics [17]. The contact number at jamming, z_J, and ϕ_J are inextricably linked to the interparticle friction in dense packings. Application of Maxwell's isostatic criterion to a frictionless hard sphere system at $\phi_J = 0.64$ reveals that $z_J = 6$. Incorporating μ between colloids further reduces ϕ_J and z_J [18,19]. The rotational constraint μ is featured in several constitutive equations, particle simulations, and phenomenological models that describe shear thickening as due to particles undergoing a stress-induced lubricated-to-frictional transition beyond σ^* [20-22]. Additionally, experimental measurements demonstrate that the rotational dynamics of shape-symmetric particles with protrusions deviate significantly from simulations of hard sphere suspensions [23-26]. While the interparticle friction may not always track with surface roughness because of complex tribological factors (*e.g.*: elastohydrodynamics [27,28]), in general, rougher particles have larger values of μ.

To investigate the role of friction on the contact microstructure of shear thickening colloidal suspensions, we use confocal rheometry experiments and dissipative particle dynamics (DPD) simulations to identify a quantitative link between the strength of thickening $\beta = \log(\Delta\eta)/\log(\Delta\sigma)$ and the distance from jamming $(\phi_{max} - \phi)/\phi_{max} = \Delta\phi/\phi_{max}$ for smooth and rough colloids. Physically, the parameter β describes the ensemble average change in suspension microstructure associated with the applied stress. Here, ϕ_{max} refers to the maximum jamming fraction for a disordered packing, where $\phi_{max} = \phi_J(\sigma = 0$ Pa) is obtained from confocal microscopy performed on colloids that have undergone unperturbed sedimentation under gravitational stress for three months. We obtain β using the average slope at the inflection points above σ^* and before the high shear plateau. At ϕ_{max}, the suspension is considered mechanically rigid and the suspension is not flowable at or beyond this ϕ. The value of ϕ_{max} is verified independently within an experimental uncertainty of ± 5% by fitting the relative low-shear viscosity ($\eta_{r,low\text{-}shear}$) divergence to the form $\eta_{r,low\text{-}shear} = (1 - \phi/\phi_{max})^{-2}$. The value of ϕ_{max} is a key parameter in normalizing the jamming distance because it varies for colloids with different surface morphologies.

We hypothesize that there is a universal correlation between $\Delta\phi/\phi_{max}$, β, and $\langle z \rangle$ for all suspensions exhibiting shear thickening. To reveal this relationship, we synthesize spherically symmetric and size-monodisperse PMMA microspheres with different levels of surface roughness [29]. These particles are sterically stabilized with poly(12-hydroxystearic acid) (PHSA) brushes of lengths 10 – 15 nm [30]. We prepare suspensions at $\phi < \phi_{max}$ by first centrifuging the stock suspension at a gravitation Péclet number, $Pe_g = 1500$ ($Pe_g = 4\pi a_{eff}^4 \Delta\rho g/3k_BT$), and subsequently diluting the shear jammed sediments with known volumes of index-matched solvent squalene. We obtain ϕ by imaging the fluorescent colloids with confocal laser scanning microscopy (CLSM, Leica SP8) and processing the 3D image volumes using a brightness-weighted centroid-based

algorithm [31]. Separately, steady shear rheological measurements are performed using a stress-controlled rheometer (TA Instruments DHR-2) fitted with a 50-mm sandblasted cone-and-plate geometry.

Fig. 1 shows different rheological behavior of PMMA hard colloids with two types of morphology and similar effective swollen diameters $2a_{\text{eff}}$, smooth (S, $2a$ = 1.65 μm ± 4%, Fig. 1a) and rocky (RK, $2a_{\text{eff}}$ = 1.49 μm ± 6%, Fig. 1b). Two other morphologies are also studied: slightly rough (SR, $2a_{\text{eff}}$ = 1.86 μm ± 5%) and very rough (VR, $2a_{\text{eff}}$ = 1.47 μm ± 6%) [32]. These steady shear flow curves describe the relative suspension viscosity ($\eta_r = \eta/\eta_s$, squalene viscosity η_s = 0.012 Pa·s) as a function of scaled σ. The dotted lines represent the two stress points at which we obtain <z> values from dynamic packings: one at $\tilde{\sigma} = \tilde{\sigma}_{\beta=0} < \tilde{\sigma}^*$ and the second at $\tilde{\sigma} = \tilde{\sigma}_{\beta} > \tilde{\sigma}^*$, where the overhead □ represents the stress values scaled by a_{eff}^3/k_BT. As $\tilde{\sigma} > \tilde{\sigma}^*$, the steric and lubrication layers between the colloids gives way to the solid-solid proliferation of interparticle contacts [21,33].

The suspensions transition from fully Newtonian flow at low σ and ϕ, to continuous shear thickening (CST, $\beta < 1$) at intermediate ϕ, and finally to discontinuous shear thickening (DST, $\beta \geq 1$) at high σ and as $\phi \rightarrow \phi_{\text{max}}$. Suspensions also exhibit a secondary plateau at the highest values of σ where the particles' motion is hindered by either frictional or hydrodynamic forces [11,14,19,21,34]. The onset of DST for smooth particle suspensions occurs at ϕ = 0.55 (Fig. 1a), which is similar to the values reported earlier in the literature for colloids interacting with a short-range repulsive potential [35,36].

Our data show that $\Delta\phi/\phi_{\text{max}}$ predicts β for different types of colloidal suspensions containing spherically symmetric particles. Fig. 2 shows that all colloidal suspensions obey the general scaling of the form, $\beta \sim \exp(-\Delta\phi/\phi_{\text{max}})$, where DST is present at $\Delta\phi/\phi_{\text{max}} \leq 0.1$ and CST is

found at $\Delta\phi/\phi_{max} > 0.1$. The value of β rapidly decreases at increasing $\Delta\phi/\phi_{max}$. Additional support for this correlation comes from β and $\Delta\phi/\phi_{max}$ values extracted from a number of literature studies: both experiments and simulations [11,19,22,33-35,37-40]. This scaling has significant impact in the academic and industrial communities because it enables the *a priori* estimation of β (a dynamic microstructure parameter) using $\Delta\phi/\phi_{max}$ (a static configuration parameter). The remarkable match between experiments and simulations from independent research groups suggests that there exists a direct link between the shear thickening microstructure of colloids and their respective quiescent jamming distance. This link is more clearly illustrated using the dynamic <z> values of shear thickening suspensions and their relation to $\Delta\phi/\phi_{max}$.

To characterize the contact microstructure of dense suspensions at the large applied stresses used to induce shear thickening, we use a custom confocal rheometer setup (Fig. 3a), where a stress-controlled rheometer (Anton Paar MCR 502 WESP) is directly coupled to a CLSM (Leica SP8) similar to an earlier set up in the literature [41]. Steady shear is applied to suspensions of smooth and rough colloids using a 20 mm parallel-plate top geometry and a glass coverslip at the bottom (thickness = 0.17 mm). The confocal rheometer is used to obtain 3D image volumes of dense suspensions undergoing steady shear at $\tilde{\sigma}_{\beta=0}$ ($\approx 10^2$) and $\tilde{\sigma}_{\beta}$ ($\approx 10^4$), as described in Fig. 1. Each stack of size 50 μm × 50 μm × 10 μm is imaged in under 5 s and contain ~ 10^3-10^4 particles. The suspensions contain 5 wt% photocrosslinking mixture to rapidly arrest the suspensions with ultraviolet (UV) light within 1 s [42]. To obtain the sheared microstructure, we hold the suspensions at constant stresses, at values marked in Fig. 1, for 150 s. We shine UV light (λ_{exc} = 405 nm) first and immediately drop the stress to zero (Δt = 1s), thus locking in the suspension microstructure without any relaxation of the sheared structures (Video_S1). We perform three

independent experiments and obtain image stacks from three different points in each sheared sample. All image stacks are imaged at least 15 μm above the coverslip to avoid wall effects.

The images obtained from the confocal rheometer experiments are supported using dissipative particle dynamics (DPD) simulations of bidisperse suspensions (a and 1.1a in an equal volume ratio with total number of particles N = 1000) containing smooth and rough colloids closely representing the experimental system [42]. The particle roughness is modeled by distributing asperities of length scale 0.1a on the surface of the smooth base spheres, similar to earlier simulations schemes [11,14,37,43-46]. To compare the data from simulations and experiments, we use the suspension systems with smooth and rough particles in simulations match the ϕ_{max} to suspensions with S and RK systems from the experiments, respectively. The goal is to link β to <z> to capture the contact networks responsible for the shear thickening phenomena.

Defining interparticle contact during shear thickening requires the use of two different contact criteria at $\tilde{\sigma} < \tilde{\sigma}^*$ and at $\tilde{\sigma} \geq \tilde{\sigma}^*$, because the particles undergo a transition from lubricated-to-frictional flow and the soft PHSA brush becomes compressed by the large applied stresses [37]. At $\tilde{\sigma} < \tilde{\sigma}^*$, two particles are defined to be in hydrodynamic contact if the interparticle separation is equal or less than the uncertainties that include the PHSA brush length, size polydispersity, and surface roughness [29]. At $\tilde{\sigma} \geq \tilde{\sigma}^*$, a frictional contact is defined by the average center-to-center distance between particles, $2a_{eff}$ as shown in Fig. 3b [47]. Thin layers of fluid could still be present between these frictional contacts. In DPD simulations, interparticle contacts are defined similarly for all particles and their interactions with other asperities and base particles. Experimental results are in excellent agreement with the contact microstructure obtained from DPD simulations for smooth and rough particles: the <z> values obtained from DPD

simulations fall within the error limits of the $\langle z \rangle$ values obtained from our experimental packings, as shown in Fig. 4a.

Visual Molecular Dynamics (VMD) renderings of the dynamic packings, at $\tilde{\sigma}_\beta$, from the experiments and simulations for suspensions containing smooth and rough particles at $\Delta\phi/\phi_{max}$ = 0.075 and β = 0.85 are shown in Fig. 3c-d. The renderings show the presence of space-spanning contact networks and provide a statistical view of how smooth and rough pack differently in shear thickening flows. Particles are concentrated in the compressive flow axis, in agreement with previous neutron scattering studies on shear thickening suspensions [16,48]. A first step towards constructing a mean-field description parameter of the contact microstructure formed in such networks would be possible by evaluating the relationship between the dynamic contact number at $\tilde{\sigma}_\beta$ and β for suspensions at various ϕ.

Fig. 4a shows the dynamic contact number, $\langle z \rangle_\beta$, as a function of $\Delta\phi/\phi_{max}$ for sheared suspensions of smooth and rough colloids. The dashed lines in Fig. 4a indicate that the smooth colloids, on average, requires an additional of 1.5 – 2 contacts to maintain the same β as compared to the rough colloids. The value of $\langle z \rangle_\beta$ is a function of $\tilde{\sigma}_\beta$ because the external deformation imparts an additional non-equilibrium free energy that must be minimized for steady flow [49]. To normalize the spatial effect of interparticle contacts that stem from free volume differences, we define a parameter z^* that captures the scaled contact deficit, where $z^* = (z_{J,\beta} - \langle z \rangle_\beta)/z_{J,\beta}$. Here, $z_{J,\beta}$ is the maximum possible contacts available at $\phi_{J,\beta}$, which is defined as the divergence of the viscosity at $\tilde{\sigma}_\beta$ and indicate the maximum flowable volume fraction at $\tilde{\sigma}_\beta$.

To estimate the shear-induced jamming point $\phi_{J,\beta}$ for suspensions of smooth and rough colloids, we invoke an argument that relates the divergence of η_r to $(\phi_J - \phi)$ at a given σ, where $\phi_J = \phi_J(\sigma)$. Specifically, the low-shear and high-shear viscosities are expected to diverge at ϕ_{max} and

a σ-dependent ϕ_J, respectively, with an exponent of -2 [50]. By extension, this suggests that η_r at intermediate σ should also diverge to a corresponding stress-dependent quasi-jamming point, $\phi_{J,\beta} = \phi_{J,\beta}(\tilde{\sigma}_\beta)$ with the same exponent of -2. The inset in Fig. 4b shows the scaling of the form $\eta_r \sim (\phi_{J,\beta}-\phi)^{-2}$ where $\phi_{J,\beta} = 0.61$ and 0.51 for smooth and rough colloids, respectively. The value of $z_{J,\beta}$ is then obtained by extrapolating $<z>_\beta$ at various ϕ to the respective quasi-jamming points $\phi_{J,\beta}$, where $z_{J,\beta}$ as 4.95±0.01 and 3.25±0.01 for smooth and rough colloids. Fig. 4b shows that the dynamic contact scaling takes the form $z^* \sim (\Delta\phi/\phi_{max})^\alpha$ with $\alpha = 0.95\pm0.07$. A similar scaling (α = 1.08) had been observed in 2D simulations of soft frictionless particles that are repulsive [51]. The observed power-law correlation in Fig. 4b is statistically significant with a normalized chi-squared parameter $\bar{\chi}^2 = 2.12$ and $P < .005$ [42,52].

In Fig. 1, following the dashed lines corresponding to $\tilde{\sigma}_\beta$ vertically, an increase in ϕ is associated with an increase in β, and a decrease in both $\Delta\phi/\phi_{max}$ and z^*, forming more space-spanning contacts. For a given $\tilde{\sigma}_\beta$, for each particle system, there exists a $\phi_{J,\beta}$ and corresponding $z_{J,\beta}$ beyond which there is no steady state flow. In a constant volume rheological experiment restricted by the dimensions of experimental and simulation setup, the free volume available to rearrange under shear is greater for smooth colloids than that of the rough colloids, because smooth colloids can rotate freely with little hydrodynamic resistance [23,53]. The difference in spatial constraints imposed by the restricted rotational degree of freedom in rough colloids is captured by the deficiency of nearest neighbors to their respective $z_{J,\beta}$. The universality in Fig. 4b shows that this physical mechanism for shear thickening holds for all types of suspensions and thus the parameter z^*, which is a contact network parameter that captures the distance to $z_{J,\beta}$, can be used as the manifestation of the modes of particle motion under shear.

The dynamic contact scaling $z^* \sim \Delta\phi/\phi_{max}$ (Fig. 4b) and the static packing correlation $\beta \sim \exp(-\Delta\phi/\phi_{max})$ (Fig. 2) can be combined to relate the sheared contact microstructure and the shear thickening strength as $\beta \sim \exp(-z^*)$. The results suggest that at a given β, because $\langle z \rangle$ is different for different suspension type, the force carried by each contact is different for particles of different morphologies. Earlier work on compressed hydrogel beads found that the macroscopic force, F, scales with dynamic contacts as $F \sim \langle z \rangle$ [54]. To obtain the same change in suspension stress (or β), rough particles suspensions required, on average, fewer contacts compared to smooth particle suspensions. In other words, for the same F in our systems, $F/\langle z \rangle$ for rough particle suspensions must be greater than that of smooth counterpart. We indirectly capture the force per contact through parameter z^*, which factors in the scaled contact deficit for various type of particle suspensions. Note that the contact networks found in this work would likely have different morphologies and properties from the force chains observed in previous studies [12]. The dynamic $\langle z \rangle$ values in our studies act as scalar parameters that describe the collective particle rearrangement under shear.

As a suspension shear thickens, clusters and percolated networks of particle contacts break and reform, but our study has shown that a mean-field description using dynamic $\langle z \rangle$ can connect β and $\Delta\phi/\phi_{max}$. The dynamic contact scaling may break down at ϕ values close to ϕ_{max} ($\Delta\phi/\phi_{max} \leq 10^{-2}$) due to pronounced flow instabilities [55-57] and the increase in uncertainty in z^* close to the jamming point could be due to these instabilities. Nonetheless, our study shows that the scaled jamming distance is a strong predictor for the shear thickening behavior of a broad class of colloidal suspensions.

Because force networks are likely coupled to the contact network and particle positions [58], future studies that analyze the transient network anisotropy could provide new insight as to how different types of particles carry load in flowing systems [59-61]. Athermal suspensions

[62,63] and shape-anisotropic colloids [64] have not been tested in this study, and it would be interesting to see if the proposed scaling laws hold for these materials.

We thank John Brady, Ronald Larson, Jeffrey Morris, and Abhinendra Singh for discussions, and Rakshit Jain for VMD reconstructions. This work is supported in part by the National Science Foundation (NSF CBET-1804462), the American Chemical Society Petroleum Research Fund (ACS-PRF #59208-DNI9), and North Carolina State University start-up funds.

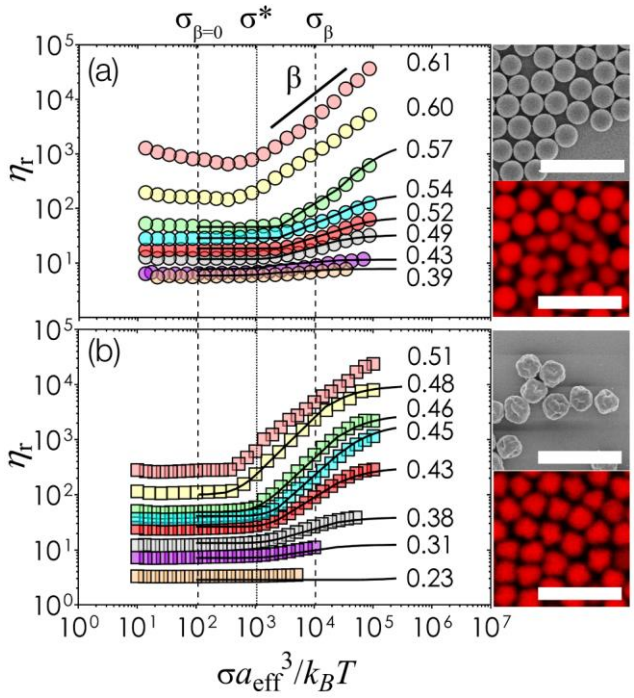

FIG 1. Experimental rheology for suspensions of (a) smooth and (b) rough colloids. Flow curves represent η_r plotted against σ scaled by the effective particle radii and temperature. Numerical values next to each curve indicate the ϕ (filled). Solid lines are fits with the WC theory [20,35,65]. The vertical dashed lines represent the stresses below and above the onset stress (vertical dotted line) where we obtain the average contact number. Representative scanning electron micrographs and confocal micrographs of colloids are shown to the right side of respective flow curves. Scale: 5 μm.

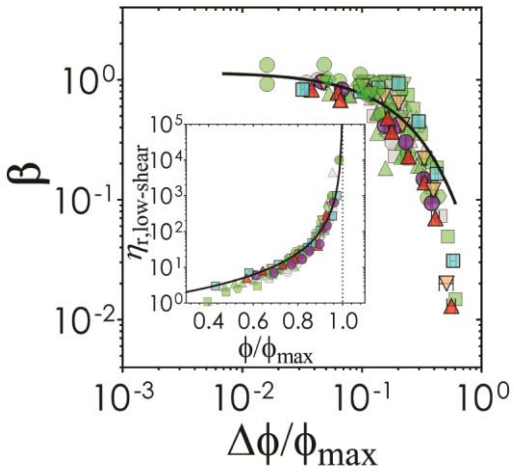

FIG 2. Shear thickening strength as a function of jamming distance. Data from this work are shown in S (magenta circles), SR (red upper triangles), VR (coral lower triangles), and RK (cyan squares) colloids. Solid line indicates an empirical fit of the form: $\beta = \beta_0 \exp(-\Delta\phi/\phi_{max}\kappa)$ with $\beta_0 = 1.61 \pm 0.05$ and $\kappa = 4.18 \pm 0.32$. Literature values from experimental colloidal studies are indicated by green symbols: smooth PMMA (circle) [35], rough PMMA (upper triangle) [37], smooth silica (square [40] and hexagon [34]), and rough silica (lower triangle [38] and diamond [39]). Literature values from simulations are indicated by grey symbols: colloids with surface asperities interacting via lubrication (square) [11], spheres with sliding friction (upper triangle) [22], spheres with sliding and rolling friction (circle) [19], and colloids interacting via sliding friction (lower triangle) [33]. Inset shows the fitting to the form: $\eta_r = (1\text{-}\phi/\phi_{max})^{-2}$ normalized for each particle ϕ_{max} values. Solid line represents the universal low-shear viscosity divergence.

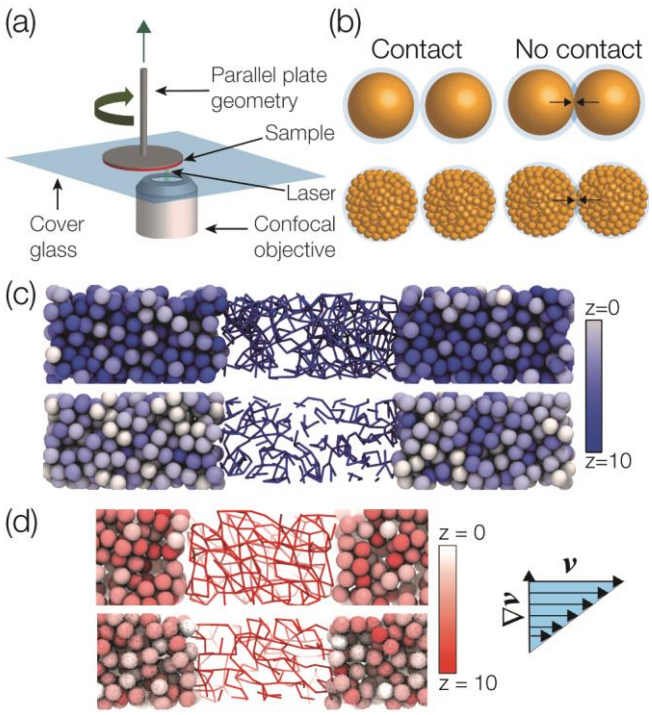

FIG 3. (a) Confocal rheometer setup for imaging shear-induced contact networks during the flow measurements. (b) Contact criterion for interparticle contact in smooth (top row) and rough (bottom row) colloids. The light blue circle represents additional experimental length scales. (c,d) Contact networks of shear thickening suspensions at $\Delta\phi/\phi_{max} = 0.075$ and $\beta = 0.85$ as shown in VMD reconstructions of the (c) experimental microstructures and (d) simulation snapshots. For (c) and (d), the top panel are for the smooth particle suspensions and the bottom panels are for rough colloidal suspensions. Side insets show color panel for the respective z of the particles shown in (c,d). Additional right inset represents the velocity-velocity gradient flow direction with respect to the contact networks shown in (c,d).

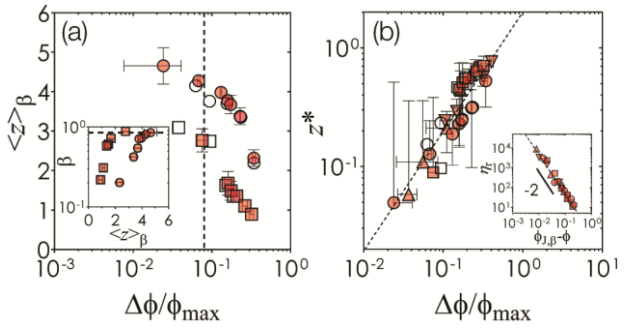

FIG 4. (a) The change in $\langle z\rangle_\beta$ of smooth (circles) and rough (squares) colloids from experiments (filled) and simulations (unfilled) as a function of $\Delta\phi/\phi_{max}$. Inset shows β as a function of $\langle z\rangle_\beta$. Dashed lines in the main figure and the inset corresponds to the suspensions at $\Delta\phi/\phi_{max} = 0.075$ and $\beta = 0.85$. (b) The scaling $z^* \sim (\Delta\phi/\phi_{max})^\alpha$ obtained from experiments and simulations. Dashed line indicates the power law fit. Inset shows the scaling relation between η_r and unscaled jamming distance to test the relation, $\eta_r \sim (\phi_{J,\beta} - \phi)^{-2}$. Two additional types of rough particles: SR (upper triangles) and VR (lower triangles) are included in (b).

References

[1] E. Blanco, D. J. M. Hodgson, M. Hermes, R. Besseling, G. L. Hunter, P. M. Chaikin, M. E. Cates, I. Van Damme, and W. C. K. Poon, Proceedings of the National Academy of Sciences **116**, 10303 (2019).

[2] E. Brown, N. Rodenberg, J. Amend, A. Mozeika, E. Steltz, M. R. Zakin, H. Lipson, and H. M. Jaeger, Proceedings of the National Academy of Sciences (2010).

[3] Y. S. Lee, E. D. Wetzel, and N. J. Wagner, Journal of Materials Science **38**, 2825 (2003).

[4] Y. Madraki, G. Ovarlez, and S. Hormozi, Physical Review Letters **121**, 108001 (2018).

[5] N. Y. C. Lin, C. Ness, M. E. Cates, J. Sun, and I. Cohen, Proceedings of the National Academy of Sciences **113**, 10774 (2016).

[6] C. S. O'Hern, L. E. Silbert, A. J. Liu, and S. R. Nagel, Physical Review E **68**, 011306 (2003).

[7] I. R. Peters, S. Majumdar, and H. M. Jaeger, Nature **532**, 214 (2016).

[8] J. F. Brady and G. Bossis, Annual Review of Fluid Mechanics **20**, 111 (1988).

[9] J. Bender and N. J. Wagner, Journal of Rheology **40**, 899 (1996).

[10] J. F. Morris, Physical Review Fluids **3**, 110508 (2018).

[11] S. Jamali and J. F. Brady, Physical Review Letters **123**, 138002 (2019).

[12] J. E. Thomas, K. Ramola, A. Singh, R. Mari, J. F. Morris, and B. Chakraborty, Physical Review Letters **121**, 128002 (2018).

[13] E. Brown and H. M. Jaeger, Reports on Progress in Physics **77**, 046602 (2014).

[14] M. Wang, S. Jamali, and J. F. Brady, Journal of Rheology **64**, 379 (2020).

[15] R. J. E. Andrade, A. R. Jacob, F. J. Galindo-Rosales, L. Campo-Deaño, Q. Huang, O. Hassager, and G. Petekidis, Journal of Rheology **64**, 1179 (2020).

[16] A. K. Gurnon and N. J. Wagner, Journal of Fluid Mechanics **769**, 242 (2015).

[17] E. Somfai, M. van Hecke, W. G. Ellenbroek, K. Shundyak, and W. van Saarloos, Physical Review E **75**, 020301 (2007).

[18] L. E. Silbert, Soft Matter **6**, 2918 (2010).

[19] A. Singh, C. Ness, R. Seto, J. J. de Pablo, and H. M. Jaeger, Physical Review Letters **124**, 248005 (2020).

[20] M. Wyart and M. E. Cates, Physical Review Letters **112**, 098302 (2014).

[21] R. Seto, R. Mari, J. F. Morris, and M. M. Denn, Physical Review Letters **111**, 218301 (2013).

[22] A. Singh, R. Mari, M. M. Denn, and J. F. Morris, Journal of Rheology **62**, 457 (2018).

[23] L. C. Hsiao, I. Saha-Dalal, R. G. Larson, and M. J. Solomon, Soft Matter **13**, 9229 (2017).

[24] S. Jiang, J. Yan, J. K. Whitmer, S. M. Anthony, E. Luijten, and S. Granick, Physical Review Letters **112**, 218301 (2014).

[25] K. V. Edmond, M. T. Elsesser, G. L. Hunter, D. J. Pine, and E. R. Weeks, Proceedings of the National Academy of Sciences **109**, 17891 (2012).

[26] L. C. Hsiao and S. Pradeep, Current Opinion in Colloid & Interface Science **43**, 94 (2019).

[27] Y. Peng, C. M. Serfass, C. N. Hill, and L. C. Hsiao, Experimental Mechanics (2021).

[28] Y. Peng, C. M. Serfass, A. Kawazoe, Y. Shao, K. Gutierrez, C. N. Hill, V. J. Santos, Y. Visell, and L. C. Hsiao, Nature Materials (2021).

[29] S. Pradeep and L. C. Hsiao, Soft Matter **16**, 4980 (2020).

[30] M. T. Elsesser and A. D. Hollingsworth, Langmuir **26**, 17989 (2010).

[31] J. C. Crocker and D. G. Grier, Journal of Colloid and Interface Science **179**, 298 (1996).

[32] D. A. Fedosov, W. Pan, B. Caswell, G. Gompper, and G. E. Karniadakis, Proceedings of the National Academy of Sciences **108**, 11772 (2011).
[33] R. Mari, R. Seto, J. F. Morris, and M. M. Denn, Proceedings of the National Academy of Sciences **112**, 15326 (2015).
[34] C. D. Cwalina and N. J. Wagner, Journal of Rheology **58**, 949 (2014).
[35] B. M. Guy, M. Hermes, and W. C. K. Poon, Physical Review Letters **115**, 088304 (2015).
[36] O. Sedes, A. Singh, and J. F. Morris, Journal of Rheology **64**, 309 (2020).
[37] L. C. Hsiao, S. Jamali, E. Glynos, P. F. Green, R. G. Larson, and M. J. Solomon, Physical Review Letters **119**, 158001 (2017).
[38] C. P. Hsu, S. N. Ramakrishna, M. Zanini, N. D. Spencer, and L. Isa, P Natl Acad Sci USA **115**, 5117 (2018).
[39] D. Lootens, H. van Damme, Y. Hémar, and P. Hébraud, Physical Review Letters **95**, 268302 (2005).
[40] J. R. Royer, D. L. Blair, and S. D. Hudson, Physical Review Letters **116**, 188301 (2016).
[41] S. K. Dutta, A. Mbi, R. C. Arevalo, and D. L. Blair, Review of Scientific Instruments **84**, 063702 (2013).
[42] See Supplemental Material at [to be inserted] for details regarding microstructure photoarresting protocol, DPD simulations, contact criterion model, and statistical analysis .
[43] A. Boromand, S. Jamali, B. Grove, and J. M. Maia, Journal of Rheology **62**, 905 (2018).
[44] S. Jamali, A. Boromand, N. Wagner, and J. Maia, Journal of Rheology **59**, 1377 (2015).
[45] A. Boromand, S. Jamali, and J. M. Maia, Computer Physics Communications **196**, 149 (2015).
[46] J. R. Melrose and R. C. Ball, Europhysics Letters (EPL) **32**, 535 (1995).
[47] R. Kubo, Reports on Progress in Physics **29**, 255 (1966).
[48] Yu-FanLee, YiminLuo, TianyiBai, C. Velez, S. C. Brown, and N. J. Wagner, Physics of Fluids **33**, 033316 (2021).
[49] V. Kobelev and K. S. Schweizer, Physical Review E **71**, 021401 (2005).
[50] M. Wang and J. F. Brady, Physical Review Letters **115**, 158301 (2015).
[51] M. Maiti, H. A. Vinutha, S. Sastry, and C. Heussinger, The Journal of Chemical Physics **143**, 144502 (2015).
[52] J. R. Taylor, *An Introduction to Error Analysis: The Study of Uncertainities in Physical Measurements* (University Science Books, Sausalito, CA, 1997), 2nd edn.
[53] A. Singh, G. L. Jackson, M. van der Naald, J. J. de Pablo, and H. M. Jaeger, arXiv:2108.09860.
[54] N. Brodu, J. A. Dijksman, and R. P. Behringer, Nature Communications **6**, 6361 (2015).
[55] G. Ovarlez, A. Vu Nguyen Le, W. J. Smit, A. Fall, R. Mari, G. Chatté, and A. Colin, Science Advances **6**, eaay5589 (2020).
[56] S. Saw, M. Grob, A. Zippelius, and C. Heussinger, Physical Review E **101**, 012602 (2020).
[57] V. Rathee, D. L. Blair, and J. S. Urbach, Proceedings of the National Academy of Sciences **114**, 8740 (2017).
[58] R. P. Behringer and B. Chakraborty, Reports on Progress in Physics **82**, 012601 (2018).
[59] M. Gameiro, A. Singh, L. Kondic, K. Mischaikow, and J. F. Morris, Physical Review Fluids **5**, 034307 (2020).
[60] L. E. Edens, E. G. Alvarado, A. Singh, J. F. Morris, G. K. Schenter, J. Chun, and A. E. Clark, Soft Matter **17**, 7476 (2021).
[61] O. Sedes, B. Chakraborty, H. A. Makse, and J. F. Morris, arXiv:2108.07261.

[62] A. Fall, N. Huang, F. Bertrand, G. Ovarlez, and D. Bonn, Physical Review Letters **100**, 018301 (2008).
[63] F. Picano, W.-P. Breugem, D. Mitra, and L. Brandt, Physical Review Letters **111**, 098302 (2013).
[64] L. Palangetic, K. Feldman, R. Schaller, R. Kalt, W. R. Caseri, and J. Vermant, Faraday Discussions **191**, 325 (2016).
[65] B. M. Guy, C. Ness, M. Hermes, L. J. Sawiak, J. Sun, and W. C. K. Poon, Soft Matter **16**, 229 (2020).